Materials Chemistry and Physics 252 (2020) 123294

Contents lists available at ScienceDirect

Materials Chemistry and Physics

journal homepage: www.elsevier.com/locate/matchemphys

Materials science communication

Enhanced photocatalytic and antifungal activity of hydroxyapatite/α-$AgVO_3$ composites

Jussara S. da Silva [a], Thales R. Machado [a,*], Aline B. Trench [a], Airton D. Silva [a], Vinícius Teodoro [a], Paulo C. Vieira [a,b], Tiago A. Martins [a], Elson Longo [a]

[a] Department of Chemistry, Federal University of São Carlos, 13565-905, São Carlos, São Paulo, Brazil
[b] Department of Physics and Chemistry, School of Pharmaceutical Sciences of Ribeirão Preto, University of São Paulo, 14040-903, Ribeirão Preto, São Paulo, Brazil

HIGHLIGHTS

- Synthesis of 7.5 and 22.5 wt% HA/α-$AgVO_3$ composites by chemical precipitation.
- Superior discoloration of MB (85%) under UV light (60 min) by 22.5 wt% HA/α-$AgVO_3$.
- HA acts as a charge carrier donor for α-$AgVO_3$, boosting the composites photoactivity.
- Photodiscoloration mainly by direct action of h^+ at α-$AgVO_3$ valence band.
- High fungistatic activity of both composites against *C. horii* and *F. guttiforme*.

GRAPHICAL ABSTRACT

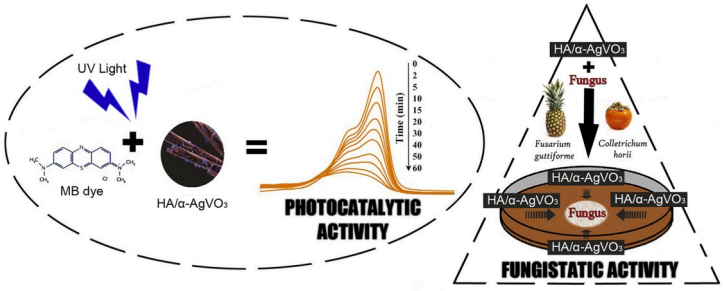

ARTICLE INFO

Keywords:
Composites
Hydroxyapatite
$AgVO_3$
Photocatalysis
Antifungal activity

ABSTRACT

Hydroxyapatite/α-silver vanadate (HA/α-$AgVO_3$) composites for fungi growth inhibition and photocatalytic discoloration of organic compounds were synthesized by chemical precipitation. The structural and morphological characterization of the 7.5 and 22.5 wt% HA/α-$AgVO_3$ composites revealed HA nanorods with hexagonal crystalline structure successfully deposited on α-$AgVO_3$ microrods with monoclinic structure. Under UV light illumination, the 22.5 wt% HA/α-$AgVO_3$ sample exhibited the highest photocatalytic activity (85%) within 60 min on the discoloration of methylene blue. A mechanism for this property is herein presented, where the main responsible for the potentialized photoactivity was the charge accumulation at the α-$AgVO_3$ band structure. Moreover, HA/α-$AgVO_3$ composites exhibited fungistatic activity against *Fusarium guttiforme* and *Colletotrichum horii*, evidencing successful preparation of multifunctional materials.

1. Introduction

Silver vanadate semiconductors, such as $AgVO_3$, Ag_3VO_4, and $Ag_4V_2O_7$ have attracted interest for environment-friendly applications in wastewater treatment due to their outstanding photocatalytic activities and biological control [1,2]. Among them, silver (meta)vanadates (α- and β-$AgVO_3$ phases) possesses narrow band gap energies and easy preparation of well crystallized phases, where β-$AgVO_3$ material was proposed for bacterial disinfection and photocatalytic degradation of organic pollutants [3]. To further increase the β-$AgVO_3$ photocatalytic

* Corresponding author.
E-mail address: tmachado.quimica@gmail.com (T.R. Machado).

https://doi.org/10.1016/j.matchemphys.2020.123294
Received 17 March 2020; Received in revised form 22 May 2020; Accepted 27 May 2020
Available online 3 June 2020

performance, heterostructures with other semiconductors were prepared, such as g-C_3N_4, $BiVO_4$, and Ag_3PO_4, rendering an improved stability, light absorption, or increasing its efficiency in charge carrier generation while avoiding their rapid recombination during photocatalysis [4].

Although less explored, α-$AgVO_3$ phase also shows potential for photocatalysis [5] and biological control [6]. Luo et al. reported that combining α-$AgVO_3$ with palygorskite lead to enhanced photodegradation activity and microorganisms inactivation [7]. However, little is known about the construction of other heterostructures containing α-$AgVO_3$ for such purposes. Hydroxyapatite ($Ca_{10}(PO_4)_6(OH)_2$, HA) efficiently adsorbs organic compounds and allows the accumulation of charge in distinct photocatalysts, including TiO_2, Fe_3O_4, and g-C_3N_4 [8,9]. These properties lead to further improvement in the overall efficiency of the composites, even in small concentrations of HA.

In this study, chemically precipitated α-$AgVO_3$ composites containing low concentrations of HA (7.5 and 22.5 wt%) nanoparticles were prepared and characterized. Their photocatalytic activities were investigated through the discoloration of methylene blue (MB). Additionally, their fungistatic properties against *Fusarium* and *Colletotrichum* species were evaluated.

2. Experimental section

2.1. Synthesis

Pure α-$AgVO_3$ and HA samples were synthesized *via* chemical precipitation [10]. To synthesize the HA/α-$AgVO_3$ composites, 7.5 or 22.5% of HA nanoparticles by weight and 1.10^{-1} mol of NH_4VO_3 (99.0%, Sigma-Aldrich) were mixed in 30 mL of distilled water. Then, another solution containing 1.10^{-1} mol of $AgNO_3$ (99.8%, Cennabras) dissolved in 30 mL of distilled water was added. The resulting precipitates were washed several times with water and ethanol, and were dried at 60 °C for 24 h.

2.2. Characterization

Phases of the products were investigated by X-ray diffraction (XRD) in a Shimadzu XRD-6000 diffractometer. Diffuse reflectance infrared Fourier transform spectroscopy was performed using a Jasco FT/IR-6200 spectrophotometer. X-ray photoelectron spectroscopy (XPS) analyses were performed on a Scienta Omicron ESCA + spectrometer. UV–Vis spectroscopy was performed using a UV 2600 (Shimadzu) spectrophotometer. The morphological features were examined by field-emission scanning electron microscopy (FE-SEM) with a Carl Zeiss Supra 35-VP microscope.

2.3. Photocatalytic activity

The photocatalytic activity was evaluated *via* photodiscoloration of MB dye. In each experiment, 50 mg of the photocatalyst was dispersed in MB aqueous solution (50 mL, 1.10^{-5} mol L^{-1}) and equilibrated in the dark. The photocatalytic test was conducted under illumination of six UV lamps (G15T8, 15 W). The MB concentrations were determined in a UV–Vis Jasco V-660 spectrometer ($\lambda = 664$ nm). Photoluminescence (PL) spectra were recorded to study the photomechanism associated to our composite samples. Spectra were collected at room temperature using a Monospec 27 Monochromator Jarrel (TermalJarrel Ash) coupled to an R955 photomultiplier (Hamamatsu Photonics). The measurements were performed with a krypton ion laser (Innova Coherente 200 K; $\lambda =$ 350 nm) as the excitation source with the incident laser beam at a maximum power of 14 mW.

2.4. Antifungal assay

The biological probes were conducted based on a recent approach to identify new potential antifungal agents [11]. For the tests, we used *Fusarium guttiforme* and *Colletotrichum horii* obtained from the microbial collection of Biological Institute of São Paulo State. Fungal axenic cultures were maintained according to Castellani method. Briefly, an inoculum of 0.5 cm in radius from each fungus was transferred from the stock to the center of a Petri dish containing sterile potato dextrose agar (PDA) medium (Acumedia). The dishes were incubated at 25 °C, in biochemical oxygen demand (BOD), with photoperiods of 12 h for 7 days. Two successive transfers were made from those dishes, and each dish was incubated under the same conditions to ensure homogeneous growth of the fungus.

An initial screening was conducted by the agar diffusion assay. An agar plate was inoculated with 1 μL of a standardized liquid culture from the fungus in PDA medium and 2 μL of the sample dispersed in sterilized distilled water (50 μg μL^{-1}). Fungus was applied 0.5 cm from the plate edge, while solution was inoculated 0.5 cm from the inoculum (1.0 cm from the plate edge). The analyzed samples were tested on the same plate. Petri dishes were incubated in BOD for 3 days, at 25 °C, with 12 h photoperiods. The experiments were conducted in triplicate.

For the agar compound incorporation assay, each experiment was performed with a water dispersion of the sample (0.5 μg μL^{-1}) in sterilized PDA Petri dishes. A 0.5 cm radius mycelium disk was transferred from the plate containing the 7-day-old fungus to the plate with the material incorporated. The plates were incubated in BOD for 4 days at 25 °C with 12 h photoperiods. Control experiments were performed using only PDA medium. All assays were performed in triplicate. Data were calculated and processed as mean ± standard deviation. Comparison analysis between groups was conducted by student's *t*-test.

3. Results and discussion

3.1. Powders characterization

Fig. 1(a) shows XRD patterns for α-$AgVO_3$, HA, and HA/α-$AgVO_3$ powders. For the pure samples, all peaks can be indexed to the monoclinic α-$AgVO_3$ structure with space group C_2/c (PDF#89-4396) and to the hexagonal HA structure with space group $P6_3/m$ (PDF#09-0432). The XRD patterns for 7.5 and 22.5 wt% HA/α-$AgVO_3$ samples were similar to that of α-$AgVO_3$, with a (002) small peak of HA structure detected for the 22.5 wt% HA/α-$AgVO_3$ sample. Fig. 1(b) shows the infrared vibrational spectra in the 1200–500 cm^{-1} region (Fig. S1 for the entire spectra). Typical bands were observed in our pure samples, including the (δ)V–O (633 cm^{-1}), (ν)V═O (654, 894, 930 and 967 cm^{-1}), (ν)V–O (775 cm^{-1}), and (ν)Ag–O–V (856 cm^{-1}) vibrational modes of α-$AgVO_3$ [10], and the (ν_2)(473 cm^{-1}), (ν_4)(564 and 604 cm^{-1}), (ν_L)(633 cm^{-1}), (ν_1)(963 cm^{-1}), and (ν_3)(1033, 1065, and 1096 cm^{-1}) modes of HA [12]. In 7.5 and 22.5 wt% HA/α-$AgVO_3$ composites, the presence of bands associated with both α-$AgVO_3$ and HA materials were observed, with an increase in intensity of HA modes as the concentration of this phase increases. These results confirm that a composite containing both phases in distinct proportions has been synthesized.

Fig. 1(c) illustrates results obtained by XPS characterization. The Ca and P main elements from HA structure and Ag and V from the α-$AgVO_3$ structure are observed simultaneously in HA/α-$AgVO_3$, with peaks associated to HA presenting higher intensity in 22.5 wt% than 7.5 wt% HA/α-$AgVO_3$ sample. The XPS spectra of Ca shows peaks at 350.6 and 347 eV related to the binding energies of Ca^{2+} $2p_{1/2}$ and Ca^{2+} $2p_{3/2}$ doublet, respectively, and the spectra for P 2p region shows a peak at 133.3 eV associated to P^{5+} of HA. The peaks related to Ag $3d_{5/2}$ and Ag $3d_{3/2}$ doublet are observed at 373.6 and 367.6 eV for Ag^+ of α-$AgVO_3$ structure, and at 374.8 and 368.8 eV for Ag^0 formed during the characterization [10]. The peaks at 524.4 and 516.7 eV correspond to the binding energies of V $2p_{1/2}$ and V $2p_{3/2}$ doublet, respectively, related to V^{5+} [13]. The optical absorption (section S1) of all samples is presented in Fig. 1(d), showing bandgap energy (*Eg*) of 2.99 and 5.45 eV for pure α-$AgVO_3$ and HA, respectively, and of 2.86 and 2.68 eV for 7.5 and 22.5

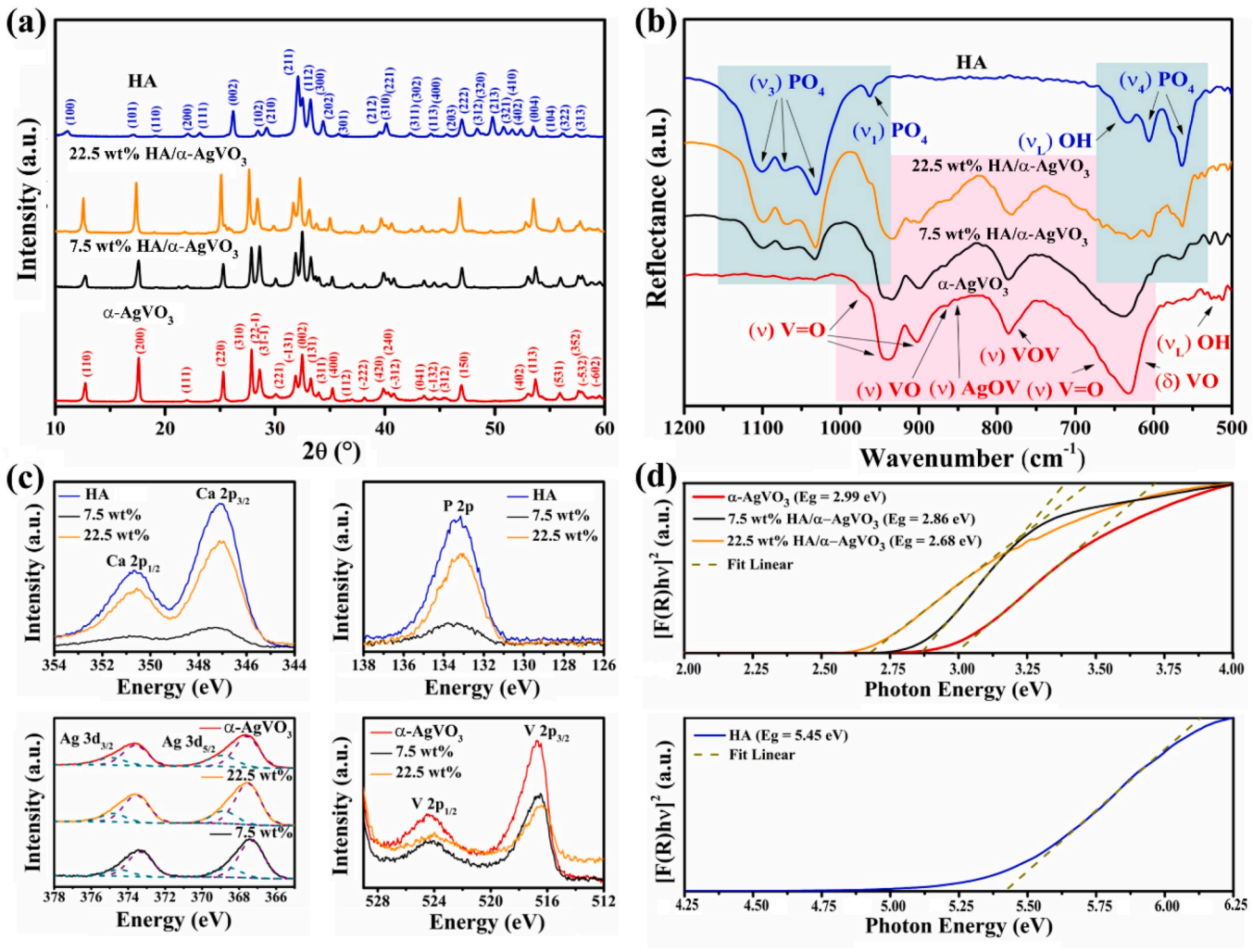

Fig. 1. (a) XRD patterns, (b) FTIR spectra, (c) XPS spectra, and (d) UV-VIS spectra.

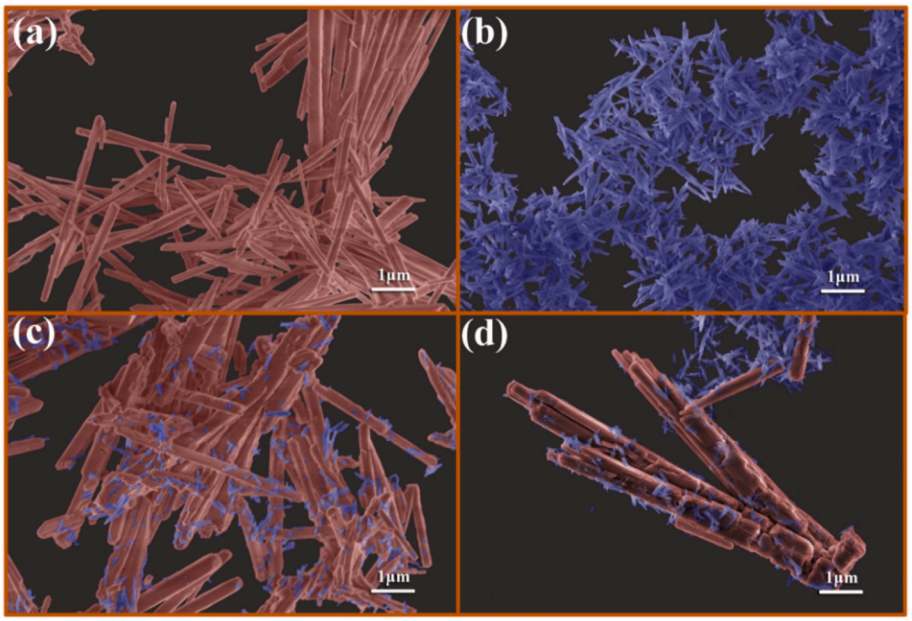

Fig. 2. FE-SEM images: (a) α-$AgVO_3$, (b) HA, (c) 7.5 wt% HA/α-$AgVO_3$, and (d) 22.5 wt% HA/α-$AgVO_3$.

wt% HA/α-$AgVO_3$, respectively.

The particle shapes for α-$AgVO_3$ (Fig. 2(a)) and HA (Fig. 2(b)) samples, determined through FE-SEM characterization, were micro- and nanorods, respectively, with sizes of 0.7 μm in width and 10.0 μm in length for α-$AgVO_3$, and 0.09 μm in width and 0.45 μm in length for HA. Fig. 2(c and d) show the results obtained for 7.5 and 22.5 wt% HA/α-$AgVO_3$, respectively, where the presence of HA nanorods partially covering the α-$AgVO_3$ microrods is observed.

3.2. Photocatalytic activity

Fig. 3(a) shows the temporal UV–vis absorption of MB probed with 22.5 wt% HA/α-$AgVO_3$ composite from 0 to 60 min (Fig. S2 for the other samples) under UV light, evidencing a significant decrease of the absorbance peak at 664 nm with time. Fig. 3(b) shows the discoloration efficiency of MB in contact with the prepared materials. The discoloration using HA (10%) is inferior to α-$AgVO_3$ (43%) over 60 min. However, by combining both materials, the resulting photocatalytic activity is significantly enhanced, reaching 65% and 85% of discoloration for 7.5 and 22.5 wt% HA/α-$AgVO_3$ samples, respectively. Fig. 3(c) shows that MB discoloration by all samples follows a pseudo-first-order kinetics. The reaction rates were 1.6×10^{-3}, 9.5×10^{-3}, 1.76×10^{-2}, and 2.99×10^{-2} min^{-1} for HA, α-$AgVO_3$, 7.5 and 22.5 wt% HA/α-$AgVO_3$ samples, respectively.

To evaluate possible causes of the higher photocatalytic activity for the composite materials, a PL analysis was conducted. The obtained results are illustrated in Fig. 3(d). The spectra of pure materials are composed by asymmetric broad band emissions centered at $\lambda = 470$ nm for HA, and at $\lambda = 726$ nm for α-$AgVO_3$ with a small shoulder at $\lambda = 460$ nm (inset in Fig. 3(d)). These emissions are typically associated to processes of radiative recombination of electron–hole (e^-–h^+) pairs encompassing countless defective energy levels localized in their respective forbidden zones [6,14].

The intense emission band at 470 nm observed for pure HA is greatly suppressed in the composite materials. It can be concluded that, in these samples, radiative recombination pathways for the photoexcited e^-–h^+ pairs at HA band structure are avoided. On the other hand, the emission profiles of the 7.5 and 22.5 wt% HA/α-$AgVO_3$ samples resemble the α-$AgVO_3$ profile (Fig. 3(d)). However, there is a progressive increase in the relative intensity of the band centered at 460 nm as well as a slight increment and shift of the emission from 726 to 696 nm in comparison to pure α-$AgVO_3$. A possible reason for such behaviors is that the HA acts as a charge carrier donor for α-$AgVO_3$ through interfacial charge carrier transfer to α-$AgVO_3$ band structure [10]. Then, the accumulated charge at α-$AgVO_3$ can radiatively recombine, as observed by the increased emission intensity of the 7.5 and 22.5 wt% HA/α-$AgVO_3$ samples in comparison to pure α-$AgVO_3$, indicating the successfully formation of a heterostructure. The photoexcited e^-–h^+ pairs accumulated at α-$AgVO_3$ band structures can also enhance the discoloration of MB dye, as observed by the photocatalytic experiments, since a higher content of electrons and holes are able to react with the adsorbed molecules.

Fig. 3(e) shows a photomechanism proposed for HA/α-$AgVO_3$ based on a straddling type of heterostructure [10]. HA possess high concentrations of intragap defective levels, allowing significant generation of e^-–h^+ pairs under UV irradiation and subsequent annihilation as photoluminescence [14,15]. However, according to the formation of straddling type of heterojunction, the differences in conduction band (CB) and valence band (VB) potentials of HA and α-$AgVO_3$ provoke an interfacial charge carriers transfer to achieve the band alignment. Hereupon, the higher CB potential of α-$AgVO_3$ compared to CB potential of HA leads to a migration of the electrons from CB_{HA} to $CB_{\alpha\text{-}AgVO3}$. Besides, the higher VB potential of HA compared to VB potential of α-$AgVO_3$ leads to a migration of electrons from $VB_{\alpha\text{-}AgVO3}$ to VB_{HA}. This latter electron transfer is understood as a migration of holes from VB_{HA} to $VB_{\alpha\text{-}AgVO3}$ since the hole mobility arises from the electron mobility. Therefore, as the HA act as a photogenerated charge carrier (e^- and h^+) donor for α-$AgVO_3$, the recombination rate of e^-–h^+ pairs in HA decreases, and there is a boost on the photocatalytic activity of α-$AgVO_3$.

In order to elucidate the improvement in the photodiscoloration mechanism for the heterostructured samples, photocatalytic

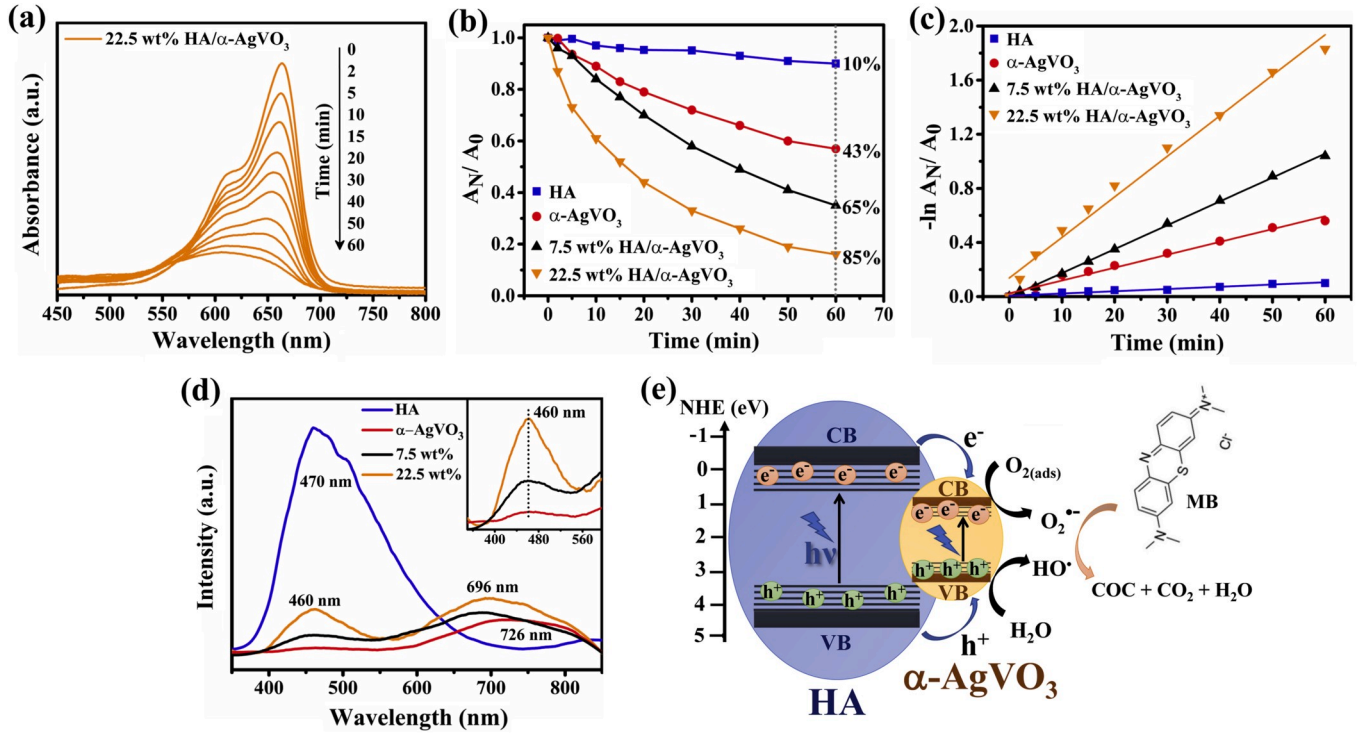

Fig. 3. (a) UV–Vis absorption of MB in solution containing 22.5 wt% HA/α-$AgVO_3$ composite, (b) discoloration efficiency, (c) first-order plot, (d) photoluminescence properties ($\lambda_{exc} = 350$ nm), and (e) photocatalytic mechanism.

experiments with reactive species scavengers were performed (Section S1 and Fig. S3). A majority action of holes for the direct photocatalytic discoloration of MB dye in comparison to their indirect action by $^{\bullet}OH$ production and the indirect action of electrons by $O_2^{\bullet-}$ production was observed. Since the electron transfer from CB_{HA} to $CB_{\alpha\text{-}AgVO3}$ is dependent of electron mobility in HA and the hole transfer from VB_{HA} to $VB_{\alpha\text{-}AgVO3}$ is dependent of electron mobility in α-$AgVO_3$, a difference in electron mobility is expected due to the different structural and electronic properties of both materials. In this sense, a possible mechanism for the observed photocatalytic results is a higher electron mobility of α-$AgVO_3$ compared to HA, resulting in a higher proportion of holes than electrons that migrate to α-$AgVO_3$. Once a fraction of photogenerated charge carriers transferred to α-$AgVO_3$ radiatively recombine, as observed by PL results, another fraction with a lower proportion of electrons than holes can reach the particle surface to react with adsorbed species. Therefore, the additional h^+ at the $VB_{(\alpha\text{-}AgVO3)}$ boosts the conversion of MB into H_2O, CO_2 and colorless organic compounds (COC), acting as the main responsible for the potentialized photocatalytic discoloration of the HA/α-$AgVO_3$ composite materials (Fig. 3(e)), with $O_2^{\bullet-}$ formed by the extra e^- at $CB_{(\alpha\text{-}AgVO3)}$ and $^{\bullet}OH$ displaying lower contributions.

3.3. Antifungal assay

The agar diffusion assay (Fig. S4) evidences high fungistatic property for HA/α-$AgVO_3$ composites. This behavior was corroborated by the agar incorporation assay, as shown in Fig. 4(a and b) for 22.5 wt% HA/α-$AgVO_3$ sample and Figs. S5 and S6 for other samples. The average mycelium growth areas in the absence (A) and in the presence (P) of the studied samples were calculated, and the obtained results are disposed in Table 1. The strongest inhibition effect was observed for α-$AgVO_3$, 7.5 and 22.5 wt% HA/α-$AgVO_3$ samples ($P < 0.05$) for both fungi analyzed.

When compared to the control groups, pure HA sample exhibited only a moderate growth inhibition against *C. horii*. On the other hand, pure α-$AgVO_3$ demonstrated a significant fungistatic activity against both tested groups. This behavior could be associated to the high capacity of α-$AgVO_3$ in generating reactive species in solution, including h^+, $O_2^{\bullet-}$, and $^{\bullet}OH$, which is in accordance with the literature [6,16]. These species can lead to the damage of cells and various cellular components through oxidative stress [17]. Although a progressive lower content of α-$AgVO_3$ is present in 7.5 and 22.5 wt% HA/α-$AgVO_3$ composites, these samples exhibited comparable results to pure α-$AgVO_3$ for both species studied. Hence, we can conclude that the fungistatic property of the overall composites departs mainly from the high capacity of α-$AgVO_3$ in generating radicals. The most relevant results were obtained for 22.5 wt% HA/α-$AgVO_3$ composite – besides its promisor fungistatic activity, this optimized sample also possesses the highest photocatalytic activity. In conclusion, these results confirm the successfully preparation of multifunctional HA/α-$AgVO_3$ composites exhibiting both photocatalytic and fungistatic properties.

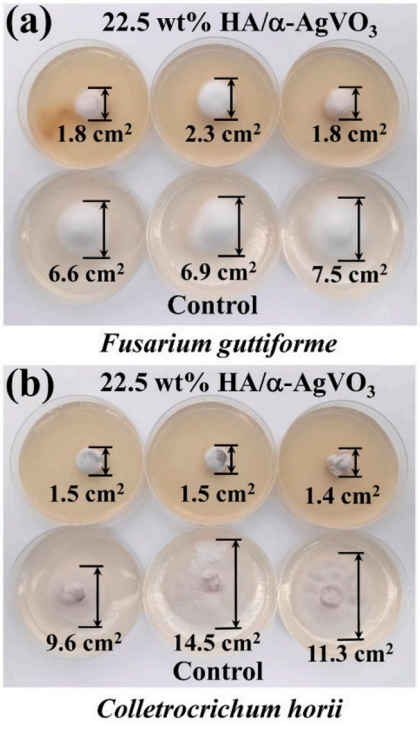

Fig. 4. Fungistatic activity of 22.5 wt% HA/α-$AgVO_3$ composite by the agar incorporation assay. Colony visual images for: (a) *Fusarium guttiforme*, and (b) *Colletotrichum horii*.

Table 1
Average mycelium growth areas of *Fusarium* sp. and *Colletotrichum* sp. in the absence (A) and in the presence (P) of the studied samples.

Treatments	Mycelium growth areas (cm^2)			
	HA	α-$AgVO_3$	7.5 wt%	22.5 wt%
Fusarium sp. growth				
A	7.0 ± 0.13	7.0 ± 0.13	7.0 ± 0.13	7.0 ± 0.13
P	14.3 ± 3.50	2.7 ± 0.04*	2.3 ± 0.07*	2.0 ± 0.08*
Colletotrichum sp. growth				
A	11.8 ± 0.72	11.8 ± 0.72	11.8 ± 0.72	11.8 ± 0.72
P	6.3 ± 0.38*	1.6 ± 0.05*	1.7 ± 0.02*	1.5 ± 0.02*

* Significant difference between A and P treatments (P values < 0.05).

4. Conclusions

Composites of HA/α-$AgVO_3$ containing distinct concentrations of HA nanoparticles (7.5 and 22.5 wt%) were successfully prepared by chemical precipitation. The photocatalytic activity probed *via* MB dye discoloration was superior for both composites in comparison to their pure counterparts, reaching 65% and 85% of discoloration over 60 min under UV illumination for 7.5 and 22.5 wt% HA/α-$AgVO_3$ samples, respectively. As indicated by photoluminescence analysis, HA acts as a photogenerated charge carrier (e^- and h^+) donor for α-$AgVO_3$. This transfer of charge carriers boosts the photocatalytic activity of HA/α-$AgVO_3$ composites, mainly by the direct action of holes accumulated at α-$AgVO_3$ valence band which react with the adsorbed dye molecules.

The fungistatic ability of our samples was evaluated by the agar diffusion and incorporation assays. Both HA/α-$AgVO_3$ composites exhibited high inhibitory effect on the growth of *Fusarium* and *Colletotrichum* species, as determined by the calculated average mycelium growth areas. The fungistatic activity of the studied materials possibly departs from their high capacities to generate reactive species in solution. Hence, despite the superior antifungal ability herein reported, HA/α-$AgVO_3$ composites also demonstrated high photocatalytic activity. These composites are promising materials for environmental remediation in removing organic contaminants and fungi growth inhibition of *Fusarium* and *Colletotrichum* species.

Declaration of competing interest

There is no conflict of interest to declare.

CRediT authorship contribution statement

Jussara S. da Silva: Investigation, Data curation, Visualization. **Thales R. Machado:** Conceptualization, Methodology, Writing - original draft, Writing - review & editing. **Aline B. Trench:** Investigation, Validation. **Airton D. Silva:** Investigation, Data curation, Writing - original draft, Writing - review & editing. **Vinícius Teodoro:**

Methodology, Writing - review & editing. **Paulo C. Vieira:** Resources, Supervision, Funding acquisition. **Tiago A. Martins:** Investigation, Validation. **Elson Longo:** Conceptualization, Resources, Funding acquisition, Supervision.

Acknowledgments

This work was financially supported by: Coordenação de Aperfeiçoamento de Pessoal de Nível Superior – Brazil (CAPES) Financial Code 001–PNPD Program, CNPq (Grant 141964/2018-9), and FAPESP (Grant 2013/07296-2). Special thanks go to Rori Camargo for technical support. The authors also thanks Prof. Maximo S. Li for the PL analyzes.

Appendix A. Supplementary data

Supplementary data to this article can be found online at https://doi.org/10.1016/j.matchemphys.2020.123294.

References

[1] R.D. Holtz, B.A. Lima, A.G. Souza Filho, M. Brocchi, O.L. Alves, Nanostructured silver vanadate as a promising antibacterial additive to water-based paints, Nanomed. Nanotechnol. Biol. Med. 8 (2012) 935–940, https://doi.org/10.1016/j.nano.2011.11.012.

[2] C.C. Chen, J. Shaya, H.J. Fan, Y.K. Chang, H.T. Chi, C.S. Lu, Silver vanadium oxide materials: controlled synthesis by hydrothermal method and efficient photocatalytic degradation of atrazine and CV dye, Separ. Purif. Technol. 206 (2018) 226–238, https://doi.org/10.1016/j.seppur.2018.06.011.

[3] T.A. Vu, C.D. Dao, T.T.T. Hoang, P.T. Dang, H.T.K. Tran, K.T. Nguyen, G.H. Le, T. V. Nguyen, G.D. Lee, Synthesis of novel silver vanadates with high photocatalytic and antibacterial activities, Mater. Lett. 123 (2014) 176–180, https://doi.org/10.1016/j.matlet.2014.03.004.

[4] J. Guo, J. Liang, X. Yuan, L. Jiang, G. Zeng, H. Yu, J. Zhang, Efficient visible-light driven photocatalyst , silver(meta) vanadate: synthesis, morphology and modification, Chem. Eng. J. 352 (2018) 782–802, https://doi.org/10.1016/j.cej.2018.07.071.

[5] T. George, S. Joseph, A.T. Sunny, S. Mathew, Visible-light photocatalytic activities of α-$AgVO_3$ nanorods and $BiVO_4$ nanobars, Int. J. Nanotechnol. 8 (2011) 963–978, https://doi.org/10.1504/IJNT.2011.044440.

[6] R.C. De Oliveira, C.C. De Foggi, M.M. Teixeira, M.D.P. Da Silva, M. Assis, E. M. Francisco, B.N.A.D.S. Pimentel, P.F.D.S. Pereira, C.E. Vergani, A.L. Machado, J. Andres, L. Gracia, E. Longo, Mechanism of antibacterial activity via morphology change of α-$AgVO_3$: theoretical and experimental insights, ACS Appl. Mater. Interfaces 9 (2017) 11472–11481, https://doi.org/10.1021/acsami.7b00920.

[7] Y. Luo, J. Luo, Y. Hua, J. Yao, S. ming Chen, X. Liu, One pot synthesis of α-$AgVO_3$/palygorskite nanocomposites with enhanced photocatalytic activity using triple roles of palygorskite: supporter, dispersant and growth-directing agent, Dalton Trans. 47 (2018) 16855–16861, https://doi.org/10.1039/c8dt02636j.

[8] C. Piccirillo, P.M.L. Castro, Calcium hydroxyapatite-based photocatalysts for environment remediation: characteristics, performances and future perspectives, J. Environ. Manag. 193 (2017) 79–91, https://doi.org/10.1016/j.jenvman.2017.01.071.

[9] T. Xu, R. Zou, X. Lei, X. Qi, Q. Wu, W. Yao, Q. Xu, New and stable g-C_3N_4/HAp composites as highly efficient photocatalysts for tetracycline fast degradation, Appl. Catal. B Environ. 245 (2019) 662–671, https://doi.org/10.1016/j.apcatb.2019.01.020.

[10] J.S. da Silva, T.R. Machado, T.A. Martins, M. Assis, C.C. Foggi, N.G. Macedo, H. Beltrán-Mir, E. Cordoncillo, J. Andrés, E. Longo, α-$AgVO_3$ decorated by hydroxyapatite ($Ca_{10}(PO_4)_6(OH)_2$): tuning its photoluminescence emissions and bactericidal activity, Inorg. Chem. 10 (2019), https://doi.org/10.1021/acs.inorgchem.9b00249 acs.inorgchem.9b00249.

[11] A. Damasceno Silva, A.R.P. Ambrozin, R.L. Carneiro, P.C. Vieira, A new approach for identifying antagonism among fungi species and antifungal activity, J. Pharmaceut. Biomed. Anal. 179 (2020) 112960, https://doi.org/10.1016/j.jpba.2019.112960.

[12] B.O. Fowler, Infrared studies of apatites. I. Vibrational assignments for calcium, strontium, and barium hydroxyapatites utilizing isotopic substitution, Inorg. Chem. 13 (1974) 194–207, https://doi.org/10.1021/ic50131a039.

[13] R. Ran, J.G. McEvoy, Z. Zhang, $Ag_2O/Ag_3VO_4/Ag_4V_2O_7$ heterogeneous photocatalyst prepared by a facile hydrothermal synthesis with enhanced photocatalytic performance under visible light irradiation, Mater. Res. Bull. 74 (2016) 140–150, https://doi.org/10.1016/j.materresbull.2015.08.028.

[14] T.R. Machado, J.C. Sczancoski, H. Beltrán-Mir, M.S. Li, J. Andrés, E. Cordoncillo, E. Leite, E. Longo, Structural properties and self-activated photoluminescence emissions in hydroxyapatite with distinct particle shapes, Ceram. Int. 44 (2018) 236–245, https://doi.org/10.1016/j.ceramint.2017.09.164.

[15] V.S. Bystrov, C. Piccirillo, D.M. Tobaldi, P.M.L. Castro, J. Coutinho, S. Kopyl, R. C. Pullar, Oxygen vacancies, the optical band gap (Eg) and photocatalysis of hydroxyapatite: comparing modelling with measured data, Appl. Catal. B Environ. 196 (2016) 100–107, https://doi.org/10.1016/j.apcatb.2016.05.014.

[16] B.N.A. da, S. Pimentel, C.C. de Foggi, P.A. Barbugli, R.C. de Oliveira, E.D. de Avila, E. Longo, C.E. Vergani, Antifungal activity and biocompatibility of α-$AgVO_3$ microcrystals: a promising material against oral *Candida* disease, Mater. Sci. Eng. C 108 (2020) 110405, https://doi.org/10.1016/j.msec.2019.110405.

[17] Z. Chen, Z. Wang, J. Ren, X. Qu, Enzyme mimicry for combating bacteria and biofilms, Acc. Chem. Res. 51 (2018) 789–799, https://doi.org/10.1021/acs.accounts.8b00011.